

Macro Flow Dynamic Study of Wind around a Gable Roof Building with Openings

Rupam Deka¹, Kalyan Kumar Das²

¹Research Scholar, Department of Energy, Assam Science and Technology University, Guwahati

²Professor, Department of Mechanical Engineering, Assam Engineering College, Guwahati

Abstract-

Understanding the flow field developed in the proximity of a building due to the wind flow over it is a prerequisite for designing a building. The wind environment around buildings plays a pivotal role not only from the point of view of structural integrity but also impacts the ventilation performance, pedestrian comfort and dispersion of pollutants. With the emergence of the green building concept in the light of the sustainable living, modern buildings are equipped with various openings such as doors, windows and ventilators. These openings change the flow characteristics in and around the building remarkably and make the flow field much more complex. The current study seeks to improve the understanding of both the internal and external flow fields around the buildings with openings. In this work, an attempt has been made to investigate the influence of wind direction on the flow behavior of wind in and around gable roof buildings with six different opening configurations. Commercially available CFD software ANSYS-FLUENT is used for numerical simulations. The numerical simulations are carried out to solve the steady Reynolds Averaged Navier Stokes (RANS) equations. The results obtained from the numerical simulations are validated with the previously published experimental results, and a good agreement was observed.

Keywords: Wind flow, Computational Fluid Dynamics (CFD), Pressure Coefficient, Suction Pressure

1. Introduction-

The flow field produced by the wind while flowing over buildings and similar structures is very complex. This flow field becomes even more complicated when the building consists of openings on its various facades. The presences of wall openings in a building significantly affect the airflow pattern and pressure distribution inside and outside the building. Therefore, detailed information on the inner and outer flow field of the buildings with openings is very much essential from the point of view of structural design, ventilation performance, pedestrian comfort and dispersion of pollutants etc.

Depending on the shape of the roof, buildings can be classified into flat roof, gable or pitched roof, hip roof, pyramidal roof, stepped roof building. Among these gable roof buildings are most common structure used for schools, hospitals, residential, commercial and industrial establishments. Due to the vast practical applications the present study focuses on understanding the inner and outer wind flow characteristics of gable roof buildings having openings on its facades.

Several studies have been carried out in the past to investigate the phenomenon of wind flow over buildings with openings. The airflow movement across a building with single opening has been investigated by [1, 2]. The phenomenon of single sided natural ventilation was studied experimentally by [3] and compared the results with a network modeling computational tool namely PASSPORT-AIR. Several experiments at Wind Engineering Research Field Laboratory (WERFL) at Texas Tech University were carried out by [4] to study the fluctuations of internal pressure due to sudden opening. They only considered single opening on the windward facade. Later on, to enhance the understanding of the impact of openings on internal pressure [5] considered another corner wall opening in addition to the windward wall opening. The Large Eddy Simulation (LES) model employed by [6] to investigate the air flow in and around a building for three different cases, including single sided ventilation with a windward opening, single sided ventilation with a leeward opening, and cross ventilation with openings on both the windward and leeward sides.

A series of experiments were carried out by [7] in a Boundary Layer Wind Tunnel (BLWT) to investigate the impact of opening area and inlet to outlet ratio on internal pressure coefficients and discharge coefficients in a building with wind driven cross ventilation. The airflow rate for a single sided opening is much lower than two sided opening; therefore [8] used some passive techniques to increase the airflow rate passing through an opening. Wind tunnel experiments were carried out and the exchange of air was measured using a constant injection rate tracer gas technique. With an aim to establish CFD as an alternative tool for studying natural ventilation analysis, [9] evaluated how accurately it can replicate the experimental results. A detailed study was carried out by [10] on the internal airflow patterns in cross ventilated buildings and tried to establish its relationship with the design and placement of openings on the building facade. Experiments were conducted at the wind tunnel employing an advanced experimental method based on PIV. The effects of physical and numerical diffusion on cross-ventilation flow in different building configurations were evaluated by [11]. The large eddy simulation (LES) model was used by [12] to investigate the influence of building length on the airflow rate in cross ventilation flow. The cross ventilation flow characteristics in sawtooth roof buildings were systematically investigated by [13, 14]. The airflow behavior in a building where two openings are located on the same wall was studied experimentally by [15]. The impact of incoming ABL velocity profile on the wind induced flow around a cubic building model having vertical openings on two opposite faces of the model was experimentally investigated by [16]. The impact on the pressure distribution in a gable roof building due to the presence of openings at various positions and different wind directions studied by [17] both experimentally and numerically. The airflow features inside a naturally ventilated dairy barn was investigated experimentally by [18]. The study basically focused on the impact of opening sizes and its locations on the indoor airflow field in an animal occupied zone (AOZ). The cross-ventilation flow through a generic building situated in a dense urban environment was analyzed by [19]. Both the indoor and outdoor flow field was investigated for various wind directions. As CFD is becoming very popular these days using the suitable numerical model is crucial for accuracy of the results. To this end [20] compared the performance of three models namely $k-\omega$ SST, Realizable $k-\epsilon$ and RNG model in predicting the wind flow over low-sloped gable roof building and found that $k-\omega$ SST perform better than the other two.

Despite the fact that an extensive research has been conducted in the past on the wind flow over gable roof buildings with openings, it appears most of them either considered single opening or openings located at opposite facades in symmetric position. A detailed study on the airflow characteristics in and around a gable roof building with openings located at asymmetric position was not conducted. The primary objective of the present work is to investigate the effect of different wind directions on the inner and outer flow characteristics of the gable roof building with openings located asymmetrically on the opposite facades. The steady RANS equations were solved using numerical simulation techniques.

2. Building Geometry and Configurations-

The size of the gable roof building model selected for the present study is 12 m × 6 m × 6 m (L×W×H), where H is the eave height of the building. The roof pitch of the building models is 5:10. Rectangular shaped openings one each on the windward and leeward façade of the building is provided. Figure-2 represents the six different building configurations obtained by locating the inlet and outlet at different vertical heights from the ground. The details of the configurations have been furnished in Table 1.

Table-1: Details of the various configurations studied

Configurations	Height of the midline of the windward opening from the ground (m)	Vertical Location of the opening on the windward facade	Height of the midline of the leeward opening from the ground (m)	Vertical Location of the opening on the leeward facade
A	4.5	Top	3	Middle
B	4.5	Top	1.5	Bottom
C	3	Middle	4.5	Top
D	3	Middle	1.5	Bottom
E	1.5	Bottom	4.5	Top
F	1.5	Bottom	3	Middle
Ref case	3	Middle	3	Middle

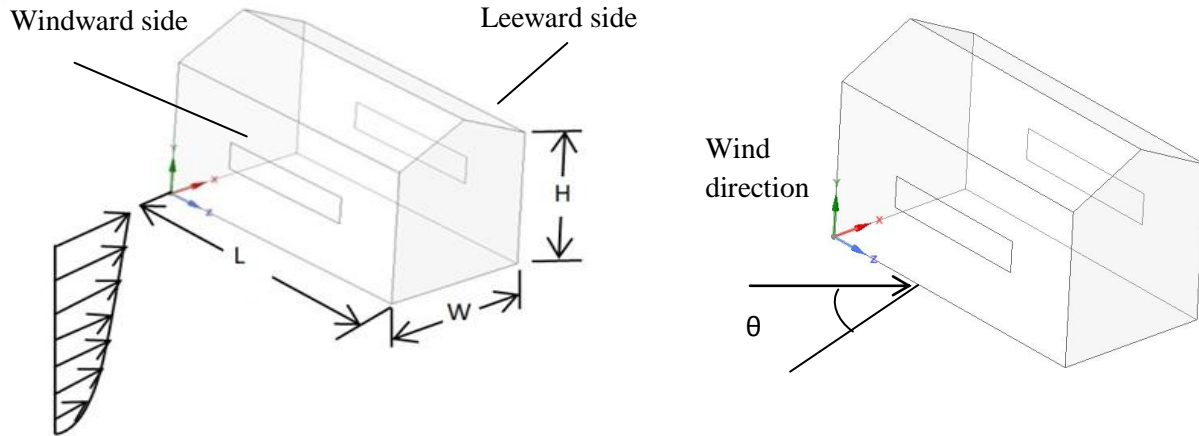


Figure-1: Geometry of the building model considered for the present study

3. CFD simulations- Settings and Parameters

3.1 Computational domain and grid

The dimensions of the computational domain were chosen based on the best practice guidelines by [21] and [22]. The upstream length was chosen as 3H instead of 5H as suggested by [23]. The resulting dimensions of the domain are 114 m × 66 m × 37.5 m (L×W×H).

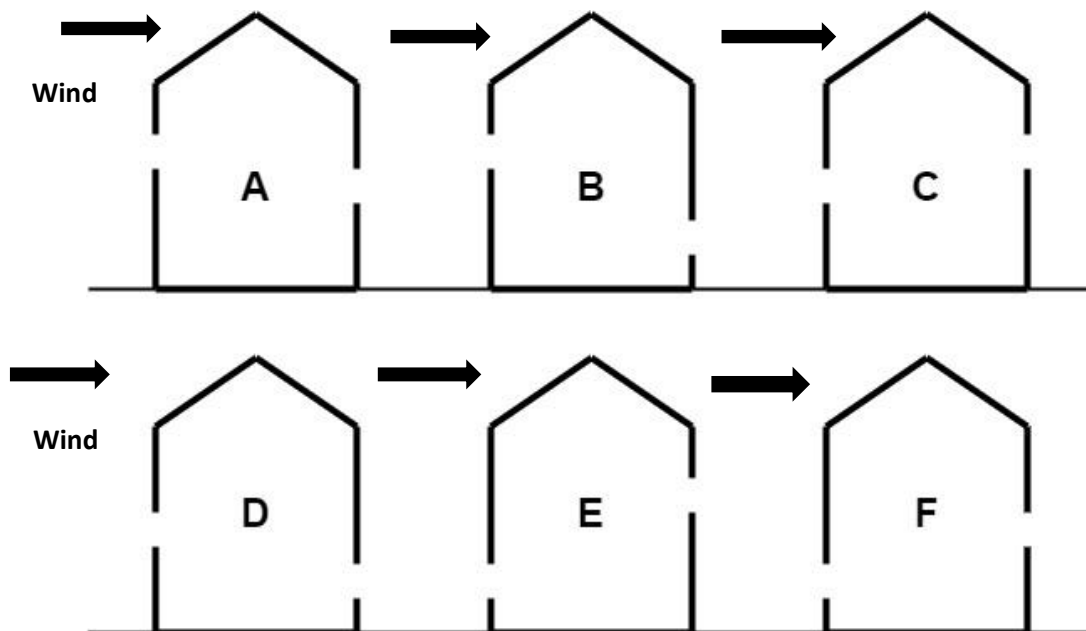


Figure 2: Cross-section of the different building configurations considered for the study

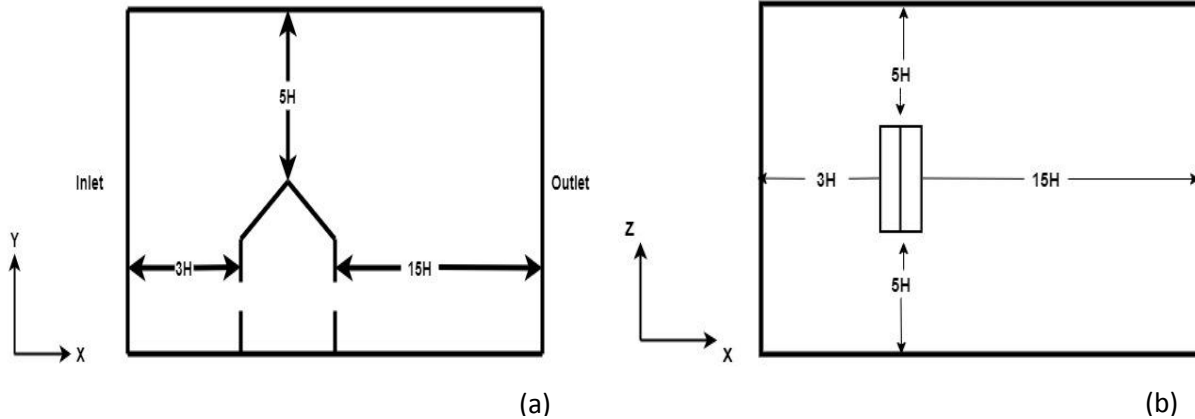


Figure-3: Dimension of the computational Domain (a) elevation of the domain (b) plan view of the domain

In the present study, a hybrid mesh was generated in the computational domain where tetrahedral elements were used near the building, hexahedral elements away from the building and near all the solid boundaries prism elements were used to capture the boundary layer developed.

3.2 Boundary Conditions

The profile of the inlet wind velocity is defined according to the Equation 1

$$U(y) = \frac{u_{ABL}^*}{\kappa} \ln \left(\frac{y+y_0}{y_0} \right) \quad (1)$$

where, u_{ABL}^* ($=0.347$ m/s) is the aerodynamic boundary layer (ABL) friction velocity which can be calculated from the velocity 10 m/s (U_{ref}) at eave height ($y_{ref}=H=6$ m), κ is Von Karman constant(0.4) and y is the height coordinate and aerodynamic roughness length ($y_0=0.0001$ m).

The turbulent kinetic energy can be determined using Equation 2

$$k(y) = \frac{\sigma_u^2(y) + \sigma_v^2(y) + \sigma_w^2(y)}{2} = a (I_u(y) \cdot U(y))^2 \quad (2)$$

where, the value of ‘ a ’ was selected as 1 ($a=1$) and $I_u(y) = \frac{1}{\ln(y/y_0)}$ was assumed.

The turbulent dissipation rate is given by Equation 3

$$\epsilon(y) = \frac{u_{ABL}^{*3}}{\kappa(y + y_0)} \quad (3)$$

The specific dissipation rate in Equation 4

$$\omega(y) = \frac{\epsilon(y)}{C_{\mu} k(y)} \quad (4)$$

Where, the C_{μ} is an empirical constant taken as a 0.09.

For ground surface, the roughness constant C_s was assumed as 1 and the sand grain roughness height k_s could be determined using Equation 5 according to their relationship with aerodynamic roughness length, y_o

$$k_s = \frac{9.793 y_o}{C_s} \quad (5)$$

For building surfaces, the roughness height and roughness constant were taken as 0 and 0.5.

Symmetry boundary conditions were imposed on the sides and top of the domain with zero normal velocity and zero gradients for all variables. The outlet of the domain was imposed with zero static pressure.

3.3 Solver Settings

In the present study, the k- ω SST turbulence model was employed to solve the 3D steady RANS equations using the CFD software package ANSYS-FLUENT version 19. The SIMPLE algorithm was used for pressure-velocity coupling. The pressure interpolation is of the second order and all other transport equations are discretized by a second order upwind scheme. Convergence is assumed to be obtained when all the scaled residuals leveled off reached by a minimum of 10^{-5} for Continuity, X, Y, Z momentum and k and 10^{-4} for ω .

As also observed by [11] the simulations showed oscillatory convergence. Therefore, as an additional criterion streamwise wind speed (U) was monitored at three different points in the domain- at centre upstream and downstream location of the building. Simulations were carried out for 5000 iterations and the results were sampled and averaged over the last 500 iterations.

3.4 Grid Sensitivity test

Grid sensitivity analysis was done for a reference case (i.e. Ref case) where the centreline joining the windward and leeward opening is at the height of 3 m from ground and the roof pitch was 5:10. The numerical simulations were performed for three different grids with 2638635 cells (basic grid), 1721133 Cells (coarse grid) and 4193546 cells (fine grid). The first layer height for all the grids were chosen as 0.0006 m. The results of wind speed ratio (U/U_{ref}) along the line joining the midpoint of the windward and leeward opening is compared for the three grids. A good match was observed between the results of fine and basic grids, however the deviations for coarse grid results was very high (refer Figure-4(a)). Therefore, the further simulations were carried out based on the basic grid.

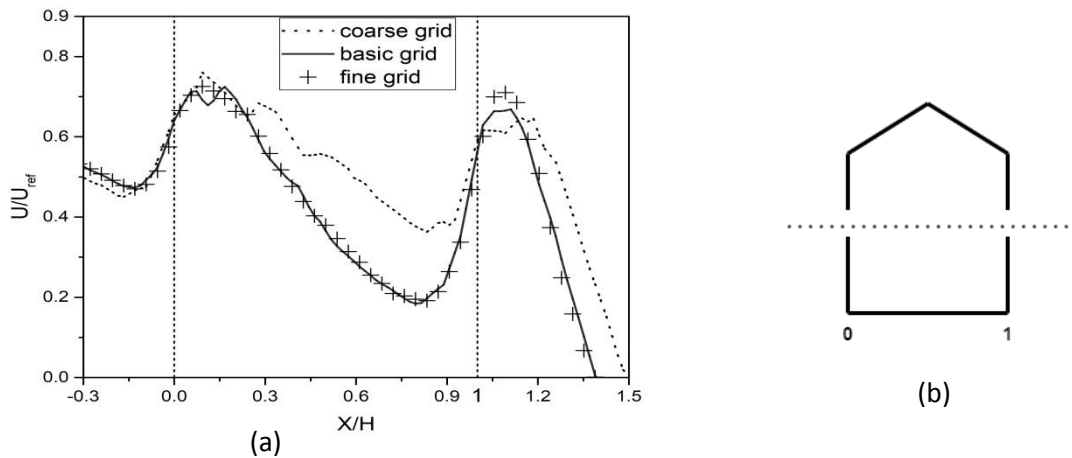


Figure-4: (a) Comparison of non-dimensional streamwise wind speed ratio for different grid resolutions (b) the model on which grid sensitivity test was done

4. CFD simulations- validation study

Validation is essential to assess the accuracy and reliability of CFD simulation results. A brief description of the validation study has been provided in this section.

4.1 Wind tunnel experiment

Particle Image Velocimetry (PIV) measurements were performed by [10] in an open circuit boundary layer wind tunnel at Concordia University in Montreal to analyze the cross-ventilation flow in simple building models. Cast transparent polymethyl methacrylate (PMMA) sheets were used to create 1:200 scale building models and had dimensions of $(W \times D \times H)$ $100 \times 100 \times 80 \text{ mm}^3$ ($20 \times 20 \times 16 \text{ m}^3$ in full scale). The openings on the windward and leeward walls were considered at three different heights: top ($h=60 \text{ mm}$), middle ($h=40 \text{ mm}$), and bottom ($h=20 \text{ mm}$), and different configurations were obtained for this study. The impact of wall porosity on cross ventilation was investigated using values of 5%, 10%, and 20%, with the height of the openings held constant at 18 mm (3.6 m in full scale) and width varied only. This paper focuses only on the configuration having openings at the middle height and with 10% wall porosity on both the windward and leeward walls. Streamwise turbulence intensity and vertical profiles of mean wind speed at the building location were measured using a hot-film probe. A reference mean wind speed $U_{ref}=6.97 \text{ m/s}$ and a streamwise turbulence intensity of 10% were recorded at building height ($H=80 \text{ mm}$), whereas the turbulence intensity was about 17% near the ground level (12 mm) and about 5% at gradient height (738 mm). An aerodynamic roughness length of $z_0=0.025 \text{ mm}$ (0.005 m in full scale) considered for this study.

4.2 Comparisons between CFD simulations and Wind tunnel measurements

The CFD simulation results were compared with the wind tunnel experiments carried out by [10]. The velocity vector field obtained from PIV measurements and numerical simulations along the vertical centre plane are presented in the Figure 6. The CFD simulations have been able to reproduce the important flow characteristics such as the standing vortex upstream of building, the flow behaviour inside the building and

the flow separation at the roof very well. The ratio of streamwise and reference wind speed (U/U_{ref}) along a horizontal line joining the midpoint of windward and leeward opening is plotted for the experimental and computed results, shown in Figure-7. Overall, good agreement between the PIV measurements and CFD simulations was observed, despite some minor discrepancies.

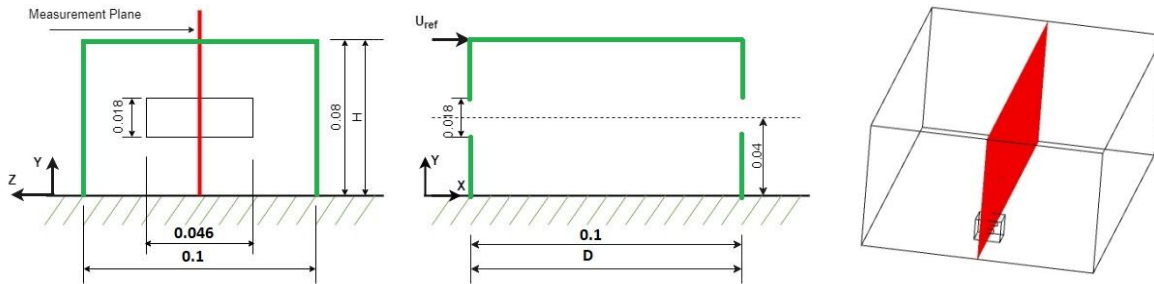


Figure-5: Model considered for the validation as studied by [10]

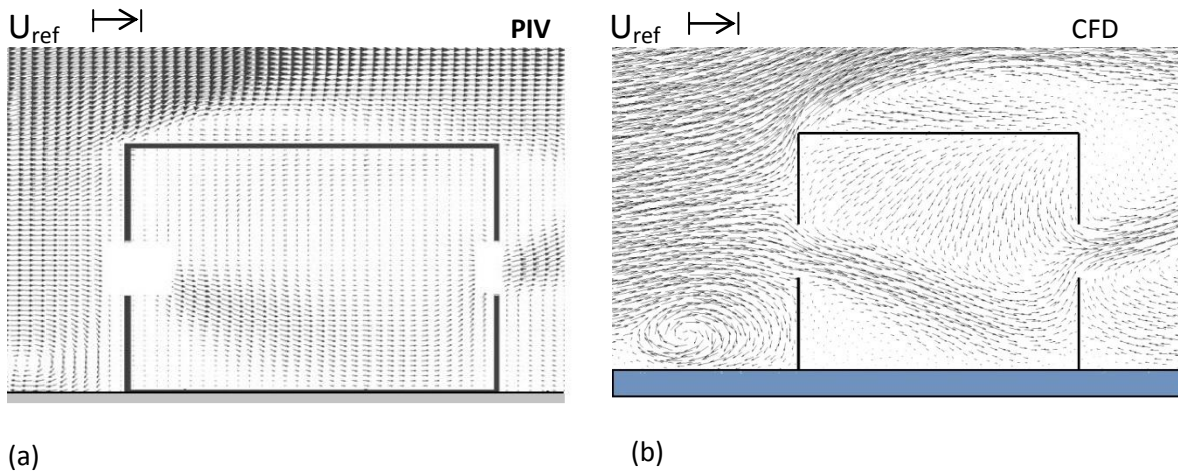


Figure-6: Comparison of velocity vector along the vertical mid-plane obtained from (a) PIV measurements done by [10]¹ (b) CFD results

¹ Reproduced from Building and Environment, 46(1), Karava, P., Stathopoulos, T., & Athienitis, A. K., "Airflow assessment in cross-ventilated buildings with operable façade elements", 266–279, copyright (2011), with permission from Elsevier.

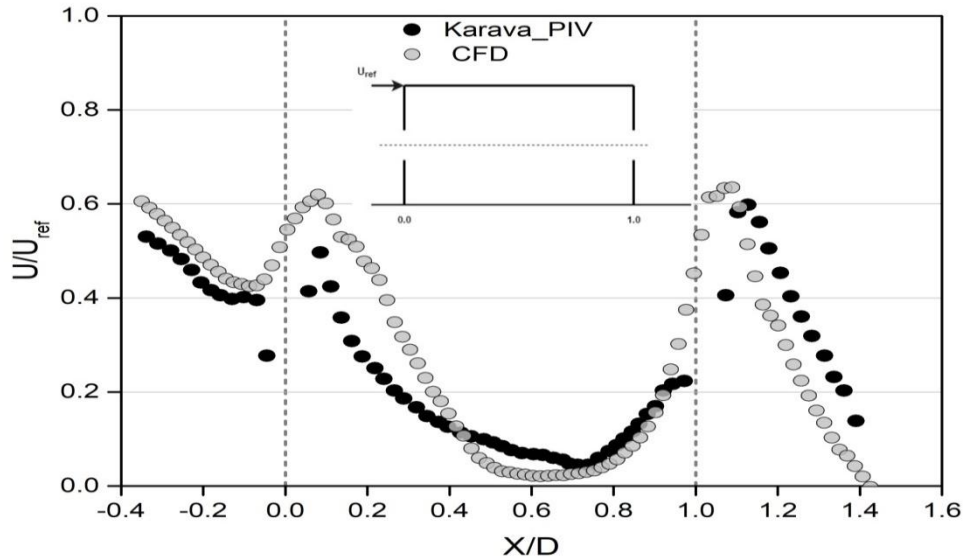


Figure-7: Comparison of non-dimensional streamwise wind velocity along the horizontal mid-line joining inlet and outlet opening

5. Results and Discussions-

In this section the impact wind direction on mean external and internal pressure of the building have been presented.

5.1 Pressure Distribution on the roof-

The pressure distributions on the roofs of various building configurations for six wind incident angles (0° , 15° , 30° , 45° , 60° , 75°) have been presented in Figures 8 to 13. In the figures, the blue region indicates the high suction area. The pressure is represented by a non dimensional term called coefficient of pressure (C_p) which is defined by Equation 6

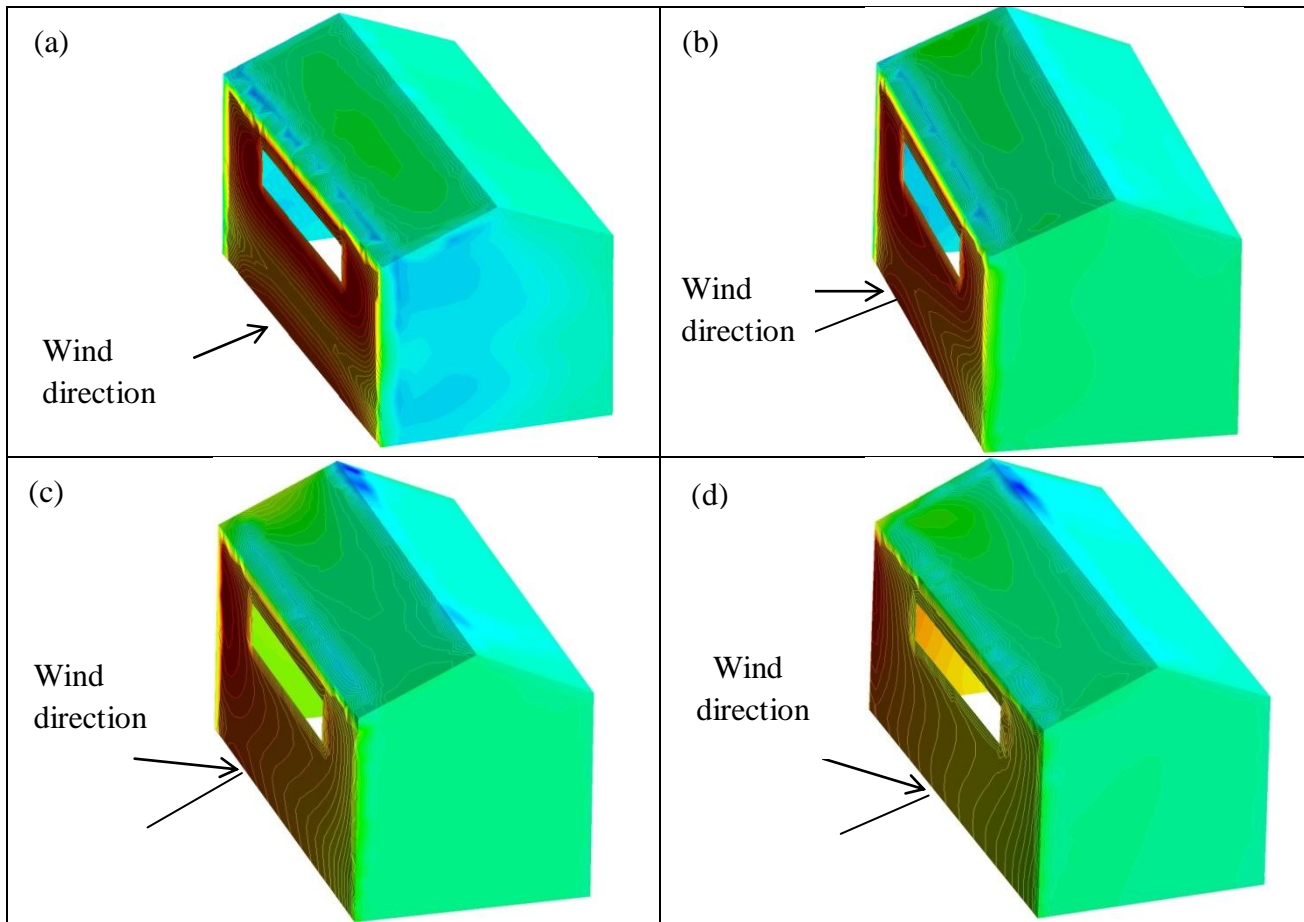
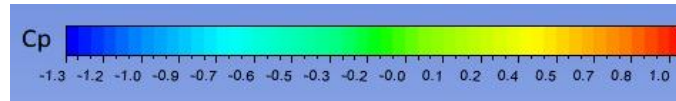
$$C_p = \frac{P - P_o}{0.5 \rho U_{ref}^2} \quad (6)$$

where, P is the static pressure, P_o is the reference pressure, ρ is the air density (1.225 kg/m^3) and U_{ref} is the reference wind velocity (10 m/s).

For all the cases tested, the high suction areas are primarily observed near the leading edge of the upwind roof (AB) and on the roof ridge (CD) due to the flow separation and formation of corner vortices. When the wind incident angle is small i.e. 0° and 15° , low pressure region is observed near the long leading edge (AB) of the upwind roof for all the configurations due to the separation of flow at the edge the upwind roof. However, for 30° and 45° wind incident angle high suction was observed towards the left of the roof ridge (CD). Further, for 60° and 75° wind attack angle low pressure region is observed on the left side of the

upwind roof. A localized very high suction region was observed on the roof ridge (CD) for the configuration F when the wind incident angle is 45° .

The results indicated that the region near the long leading edge (AB) of the upwind roof and the roof ridge (CD) are the two most critical areas of the gable roof building since high suction occurs mainly in these two areas due to the formation of roof corner vortices and separation of flow. It is to be noted that the pressure distribution on the roof of a building is strongly dependent on the relative position of the inlet and outlet openings on the building facades well as with the wind incident directions. Keeping above in view, the pressure variations along the long leading edge (AB) and the roof ridge (CD) have been studied and highlighted in the subsequent section.



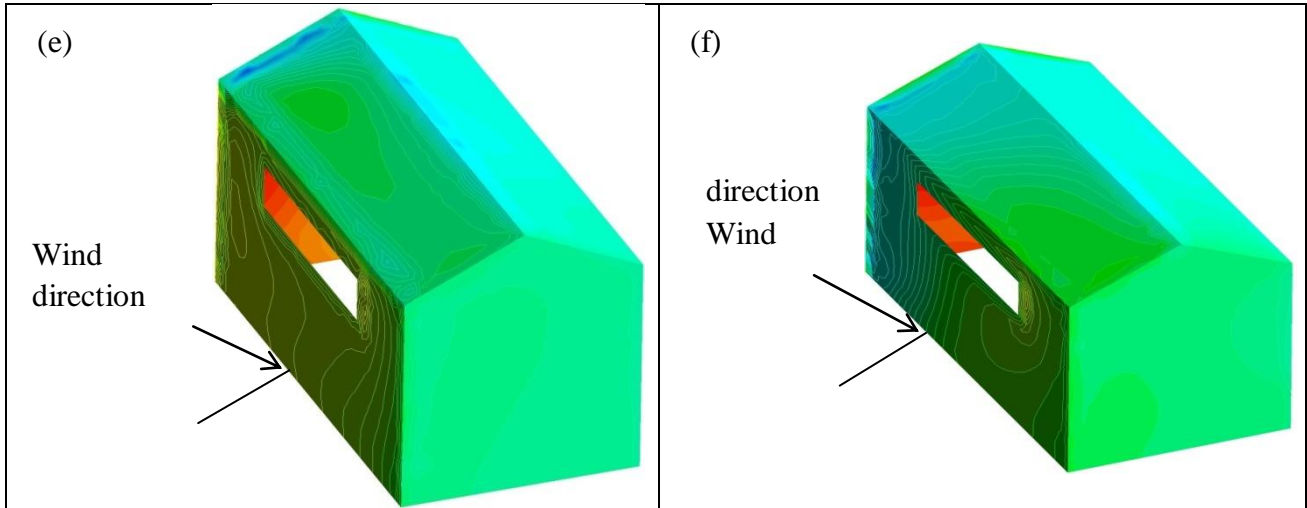
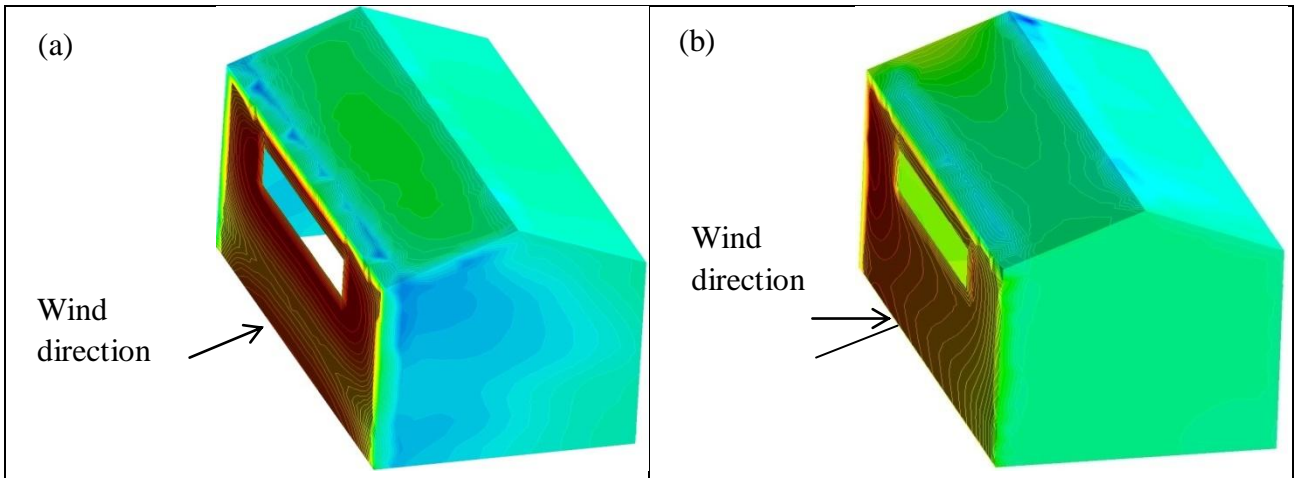
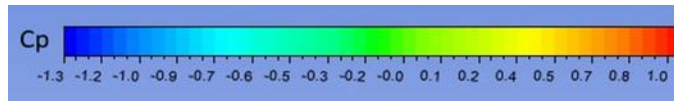


Figure-8: Pressure contours on the roof for Configuration-A for various wind directions : (a) 0° , (b) 15° , (c) 30° , (d) 45° , (e) 60° , (f) 75°



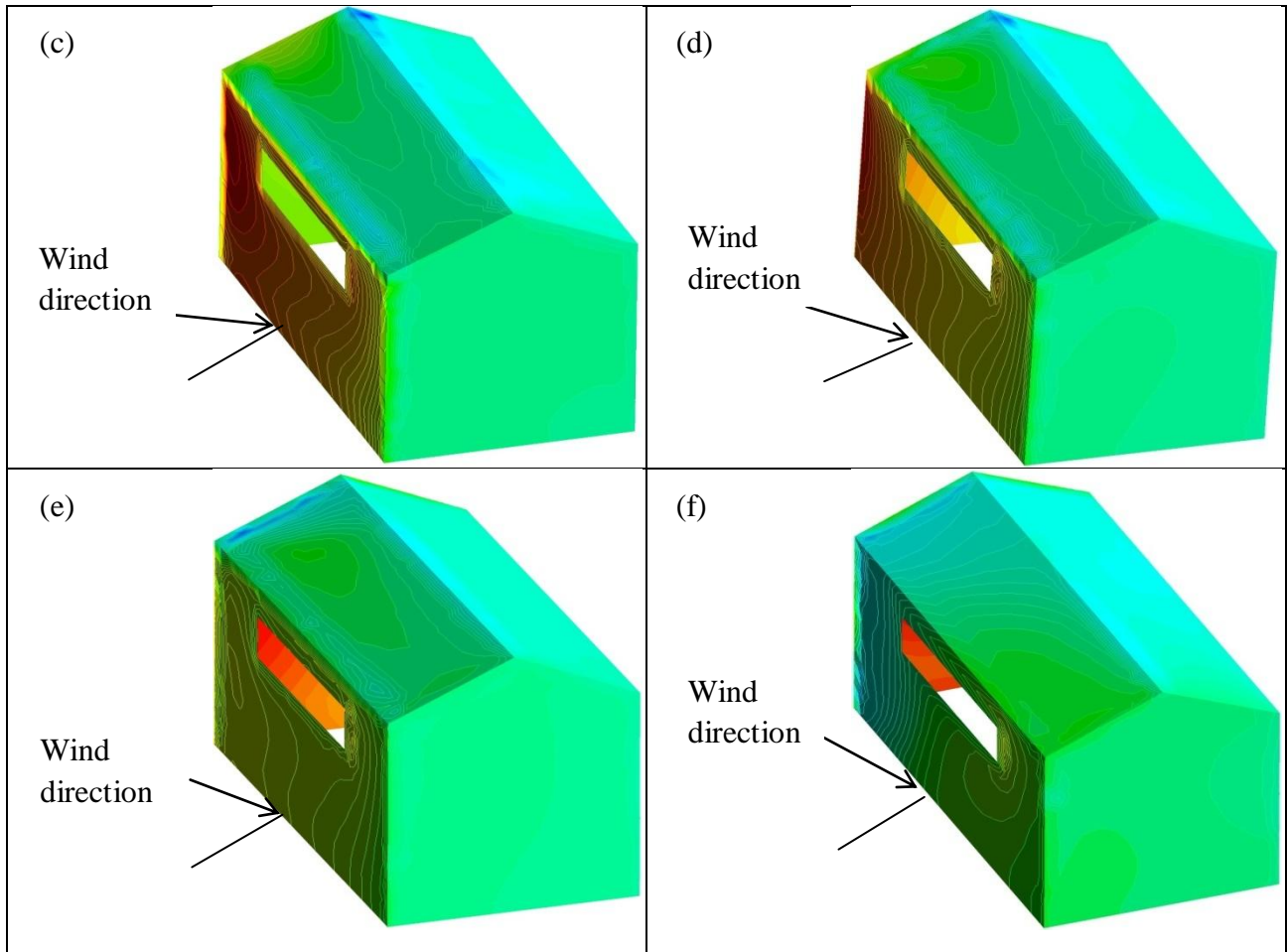


Figure-9: Pressure contours on the roof for Configuration-B for various wind directions: (a) 0° , (b) 15° , (c) 30° , (d) 45° , (e) 60° , (f) 75°

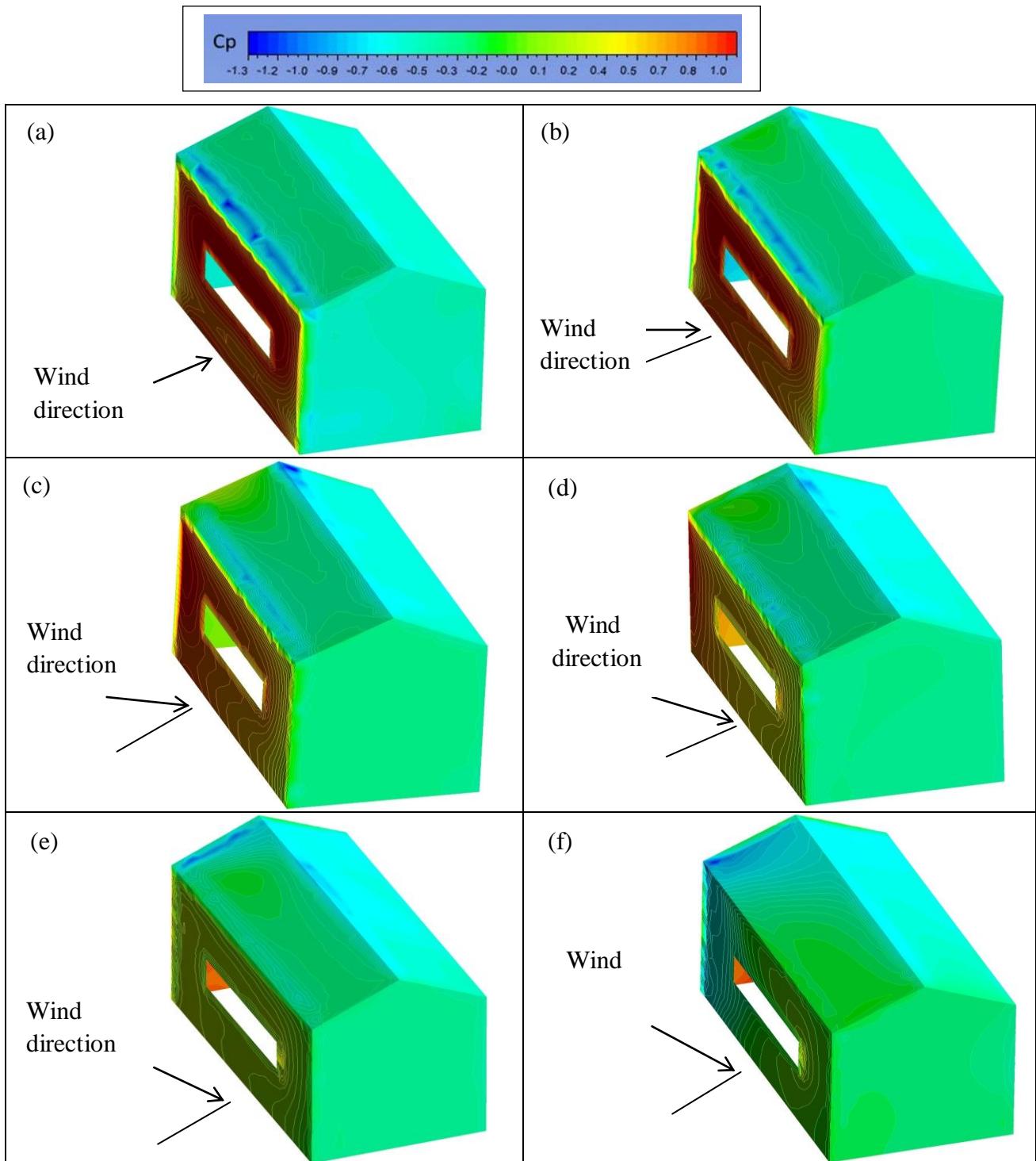


Figure-10: Pressure contours on the roof for Configuration-C for various wind directions: (a) 0° , (b) 15° , (c) 30° , (d) 45° , (e) 60° , (f) 75°

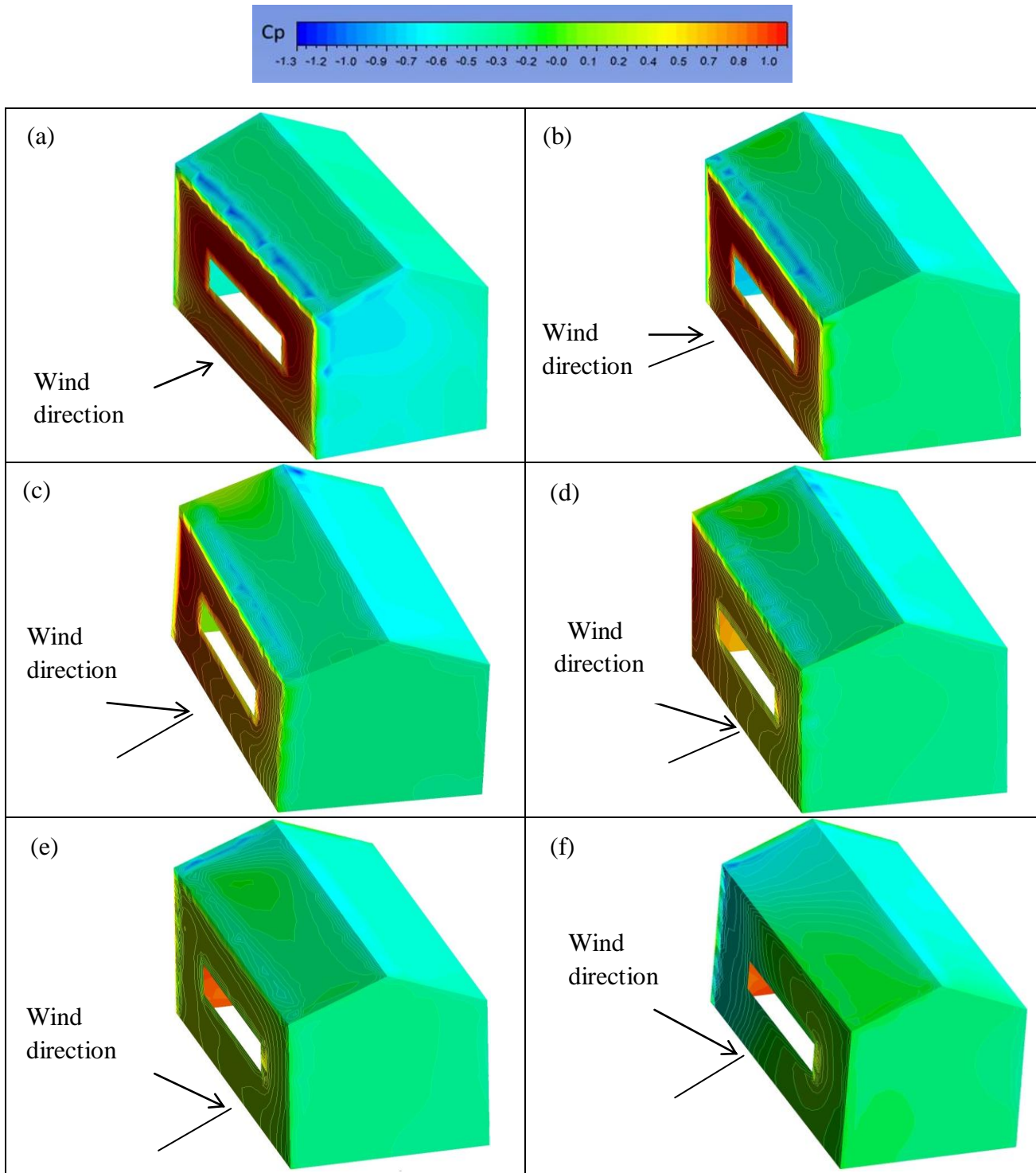


Figure-11: Pressure contours on the roof for Configuration-D for various wind directions: (a) 0°, (b) 15°, (c) 30°, (d) 45°, (e) 60°, (f) 75°

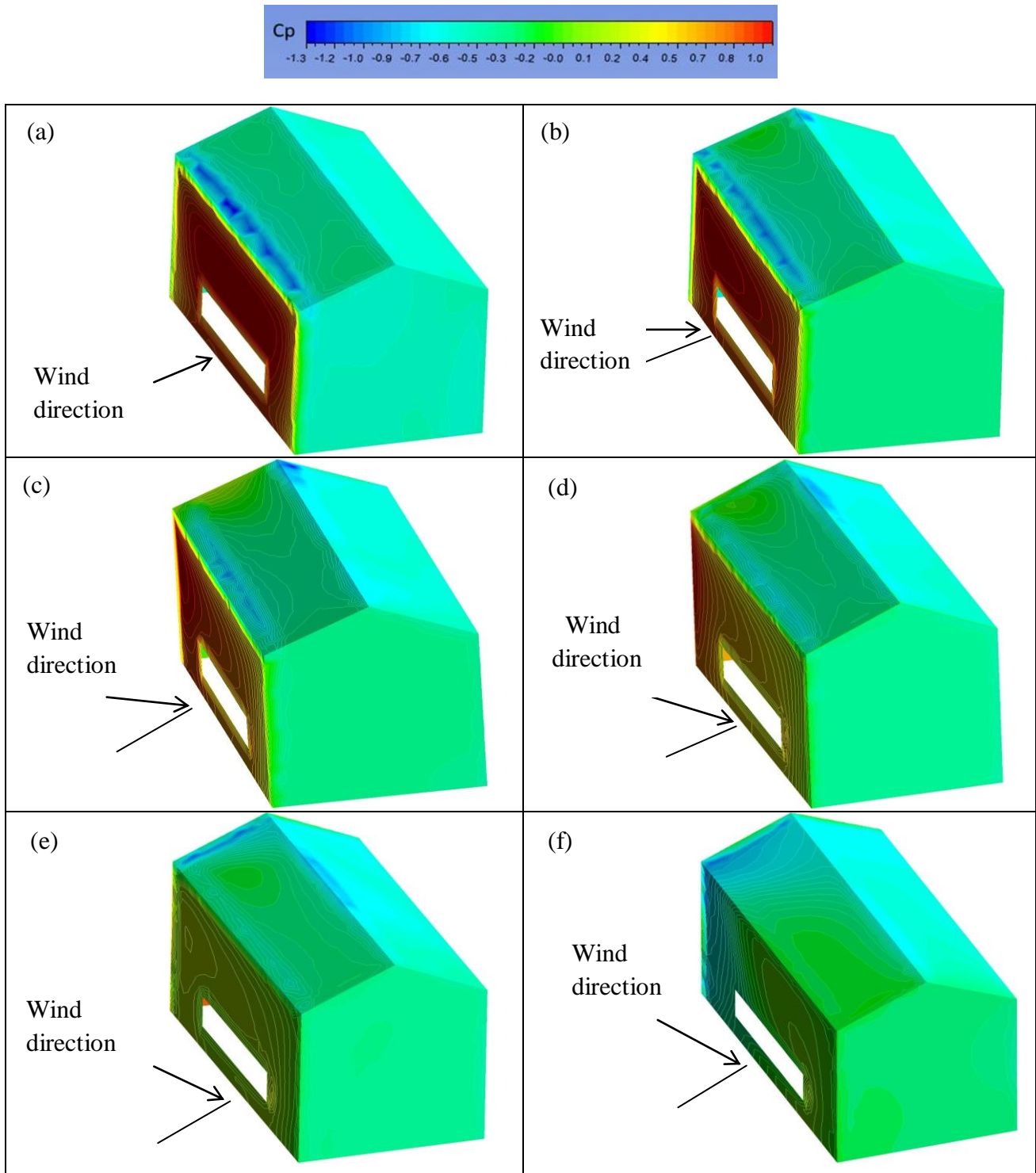


Figure-12: Pressure contours on the roof for Configuration-E for various wind directions: (a) 0°, (b) 15°, (c) 30°, (d) 45°, (e) 60°, (f) 75°

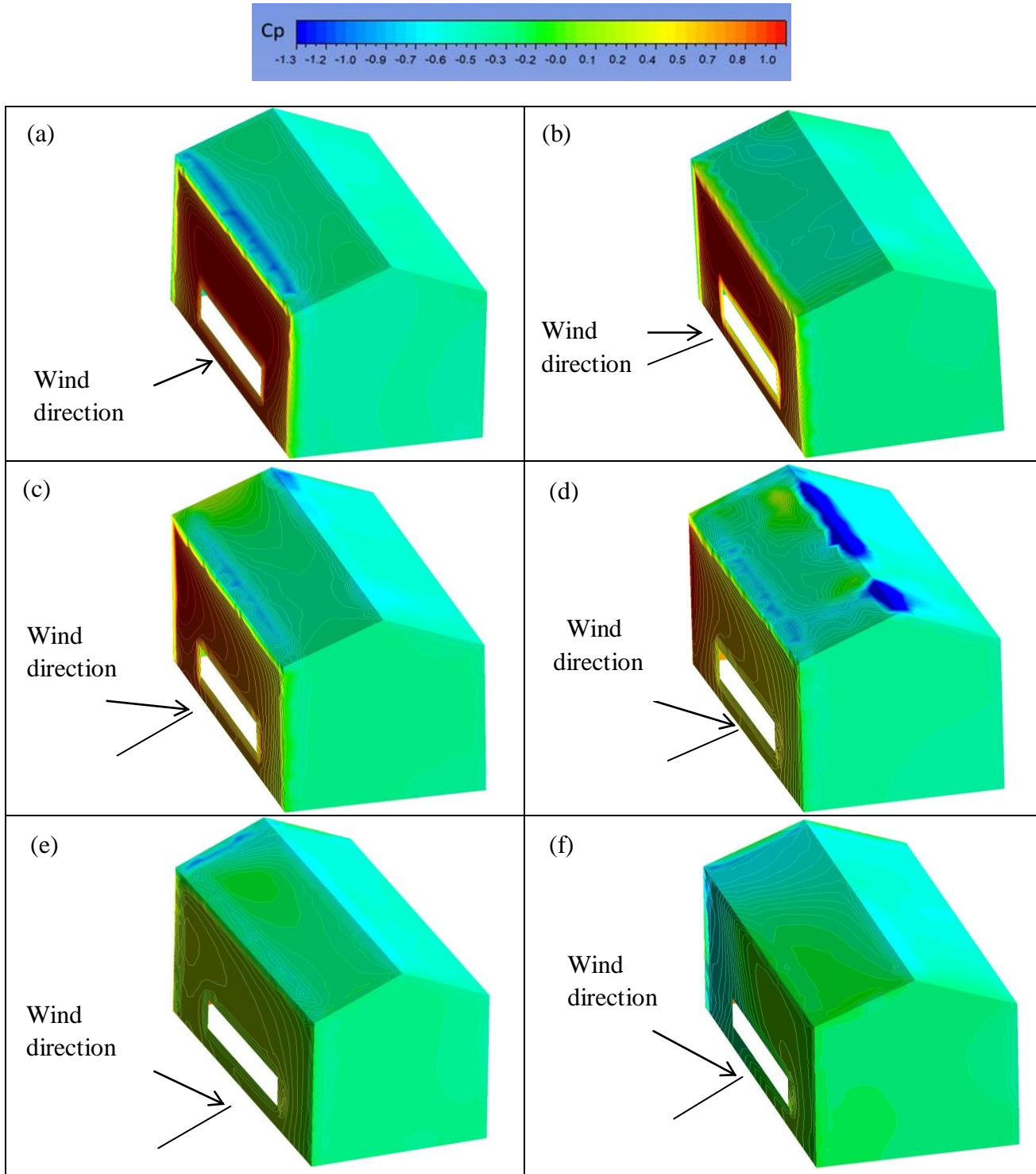
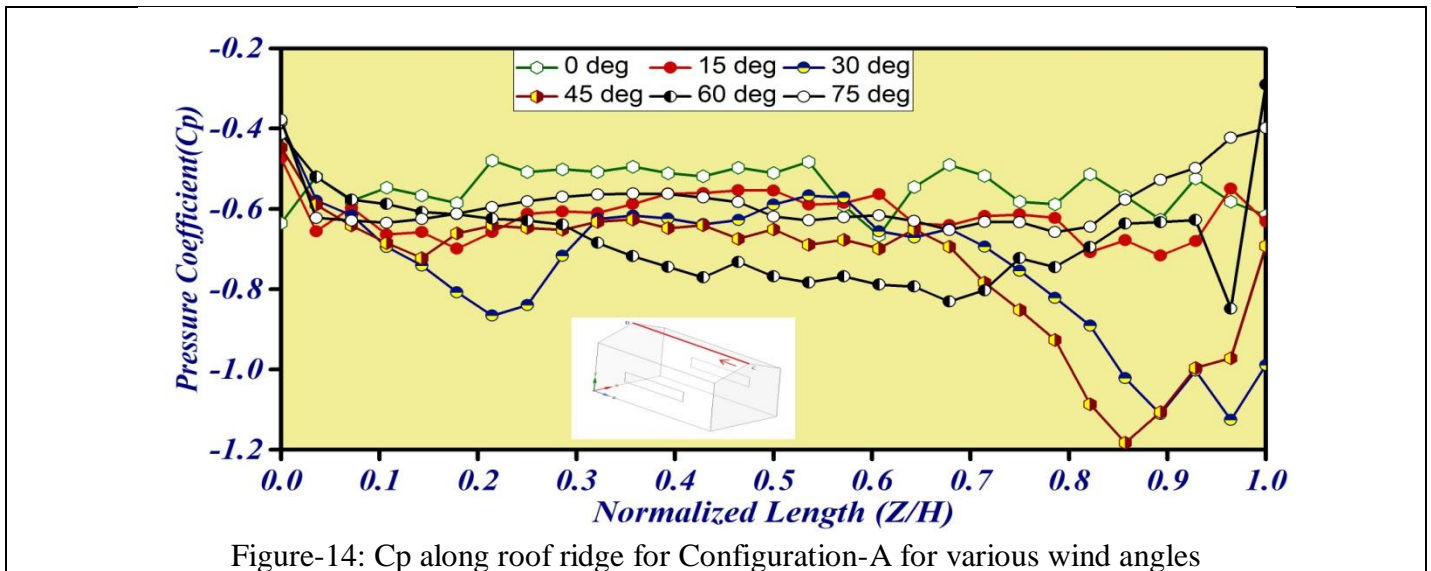


Figure-13: Pressure contours on the roof for Configuration-F for various wind directions: (a) 0°, (b) 15°, (c) 30°, (d) 45°, (e) 60°, (f) 75°

5.2 Variation of pressure along roof ridge (CD)-

In the Figures-14 to 19, the pressure distribution along the roof ridge for various configurations has been shown, wherein the pressure coefficient is represented as a function of the normalized length along the roof ridge. Irrespective of the configurations for all the wind incident directions studied i.e. (0° to 75°) the pressure on the roof ridge is negative. The location and the value of the highest suction pressure coefficient vary with the different configurations as well as the wind directions. Generally, for the configurations A to E and with all the wind incident directions the minimum C_p values were obtained towards the left end of the roof ridge (CD) however, for the configuration F, the highest negative pressure value was obtained towards the right end of the roof ridge under the wind direction 75° . For configuration A, suction pressure coefficient reaches peak value of -1.18 for 45° wind incident angle. In case of configuration B, almost similar pressure distribution was observed along the roof ridge when the wind incident directions are 15° and 30° and the highest suction pressure around -1 was obtained for these two wind directions. The highest negative pressure values of -1.1, -0.93 and -1.04 were obtained for configurations C, D and E under the wind directions 30° , 45° and 30° respectively. For the configuration F, the magnitude of the suction pressure coefficient rises to a maximum value of -2.53 when the wind incident direction is 45° . Sufficient attention is needed to this end because of the vulnerability of the building structure due to this highly localized wind pressure on the roof.



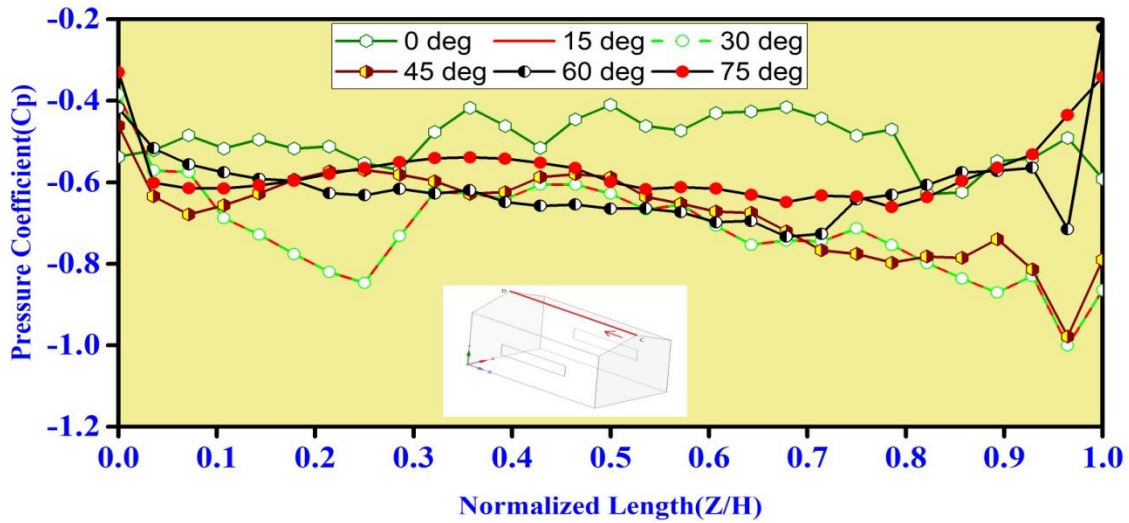


Figure-15: Cp along roof ridge for Configuration-B for various wind angles

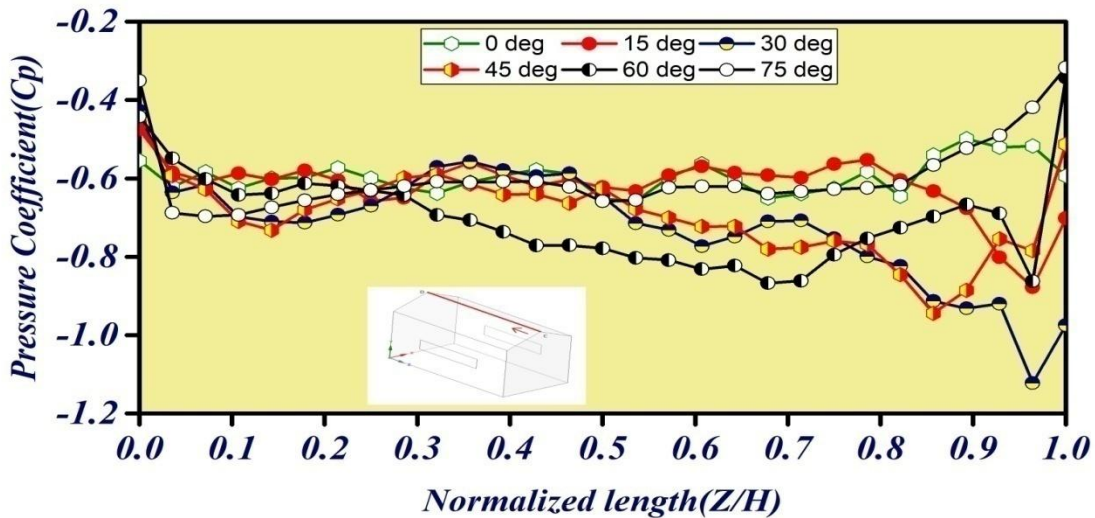


Figure-16: Cp along roof ridge for Configuration-C for various wind angles

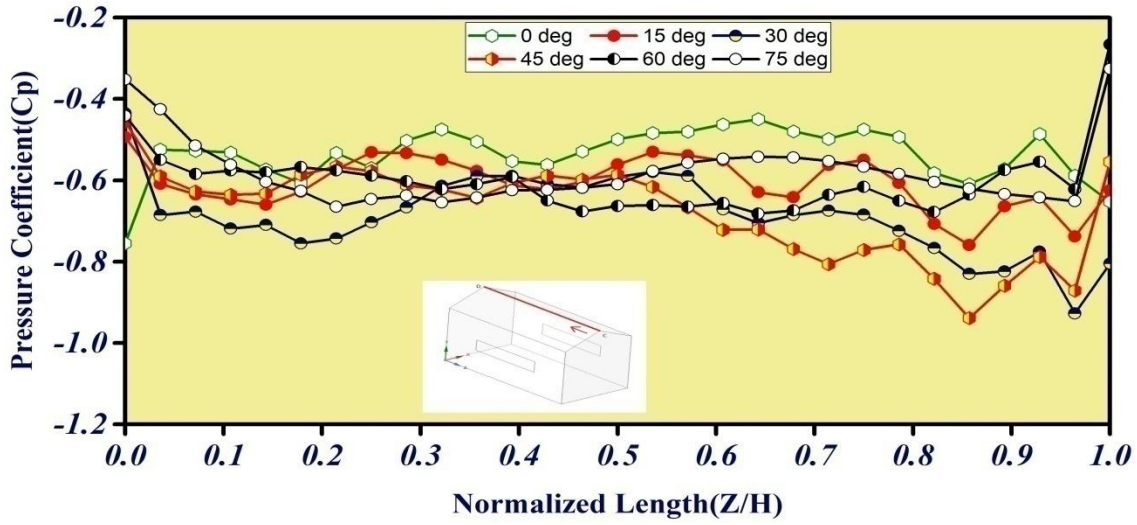


Figure-17: C_p along roof ridge for Configuration-D for various wind angles

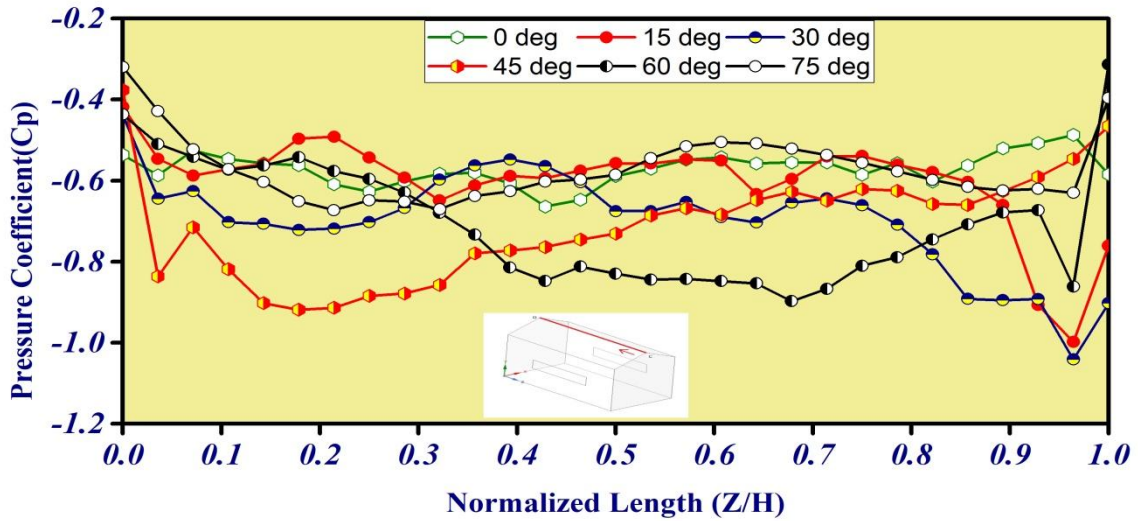


Figure-18: C_p along roof ridge for Configuration-E for various wind angles

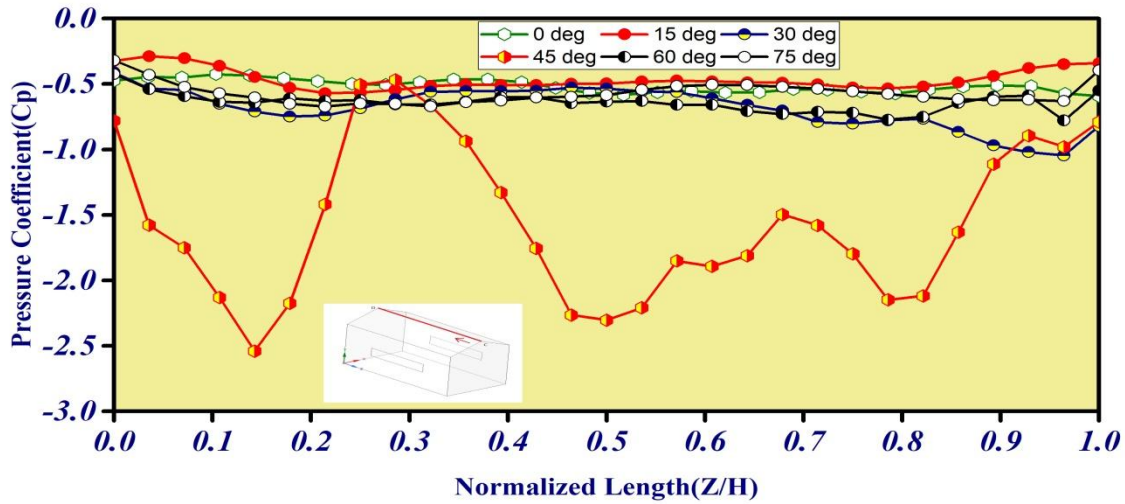


Figure-19: Cp along roof ridge for Configuration-F for various wind angles

5.3 Variation of pressure along the long leading edge (AB)-

The pressure distribution along the long leading edge (AB) was shown in Figure 20 to 25, where the normalized length along the long leading edge was chosen as the X-axis and coefficient of pressure (C_p) values were plotted along the Y-axis. The location and the minimum pressure value vary with the configurations and the wind incident angles. Along the long leading edge for all the configurations pressure values were negative for wind incident direction 0° , 15° , 60° and 75° however, towards the left side of the long leading edge positive values of pressure were found for wind incident angles 30° and 45° . It is found that the magnitude of negative pressure on the long leading edge is less significant as compared to roof ridge. For configurations A, C, E and F the suction pressure reaches peak value for wind direction 75° however, for configuration B and D magnitude of suction pressure reaches maximum value under wind direction 0° . Among the cases studied, the magnitude of the maximum suction pressure on the long leading edge reaches the value of -0.93.

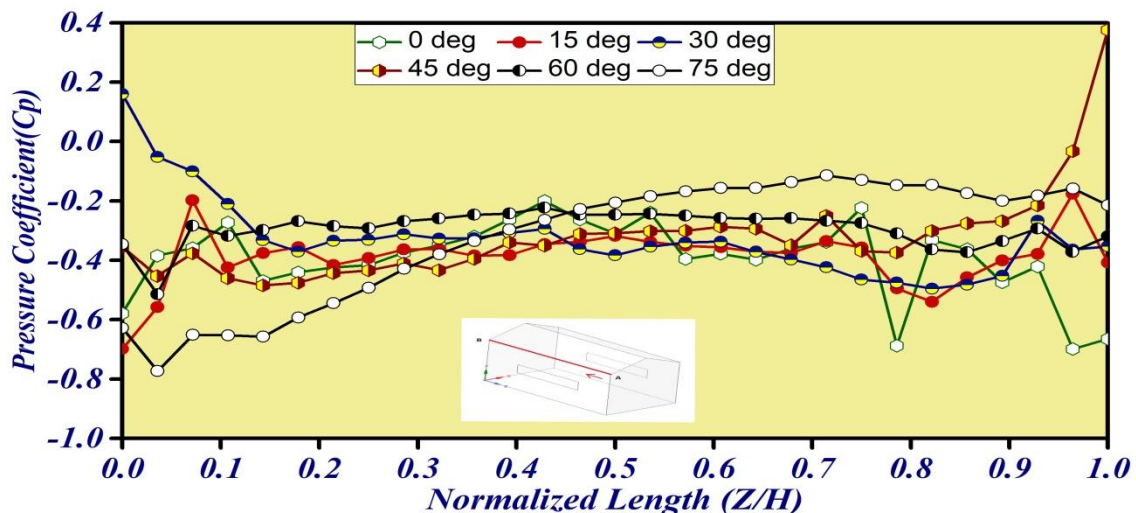


Figure-20: Cp along long leading edge for Configuration- A for various wind angles

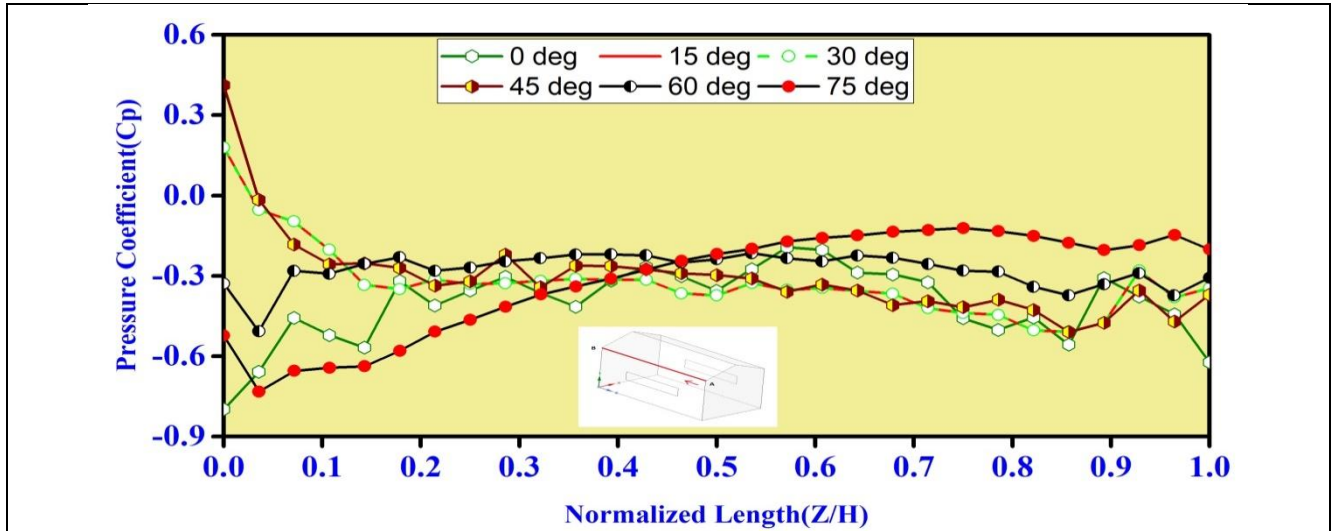


Figure-21: Cp along long leading edge for Configuration- B for various wind angles

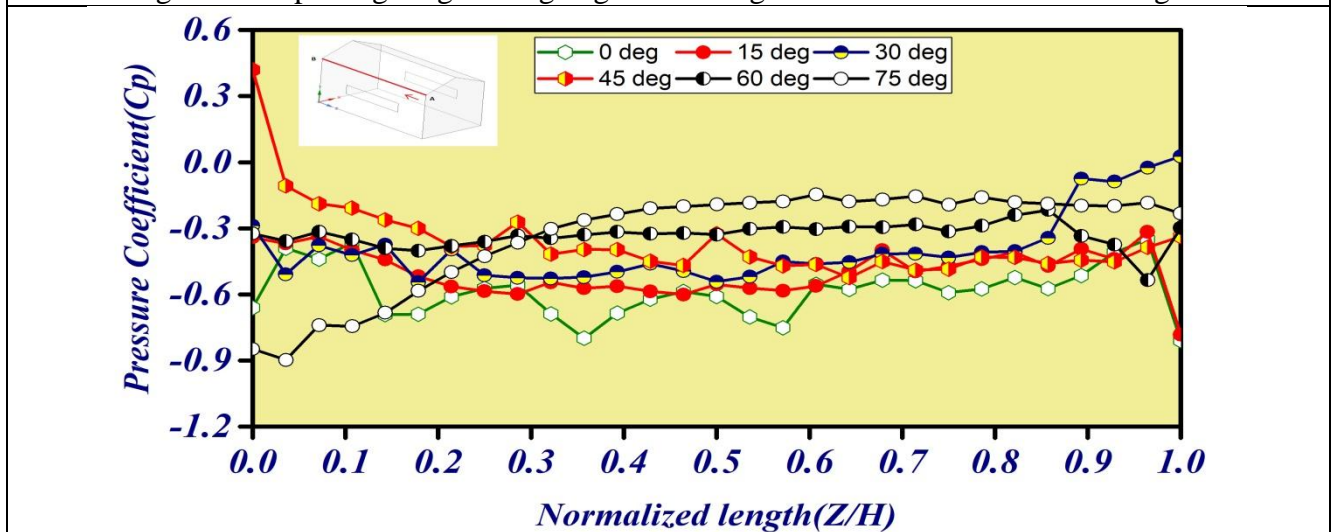
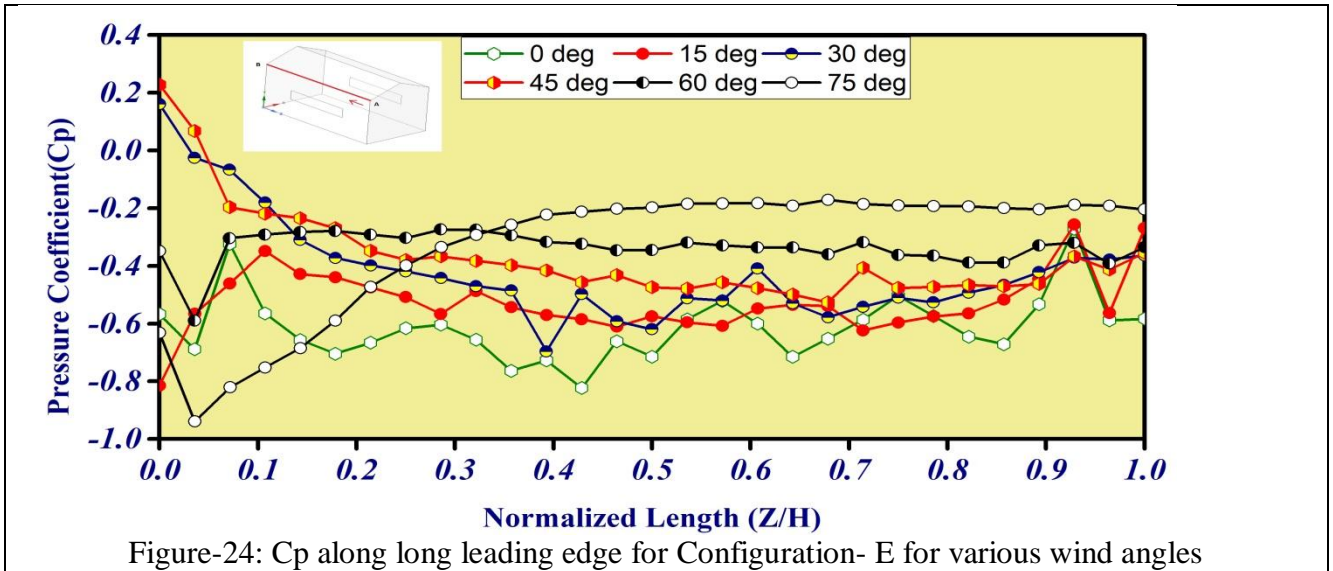
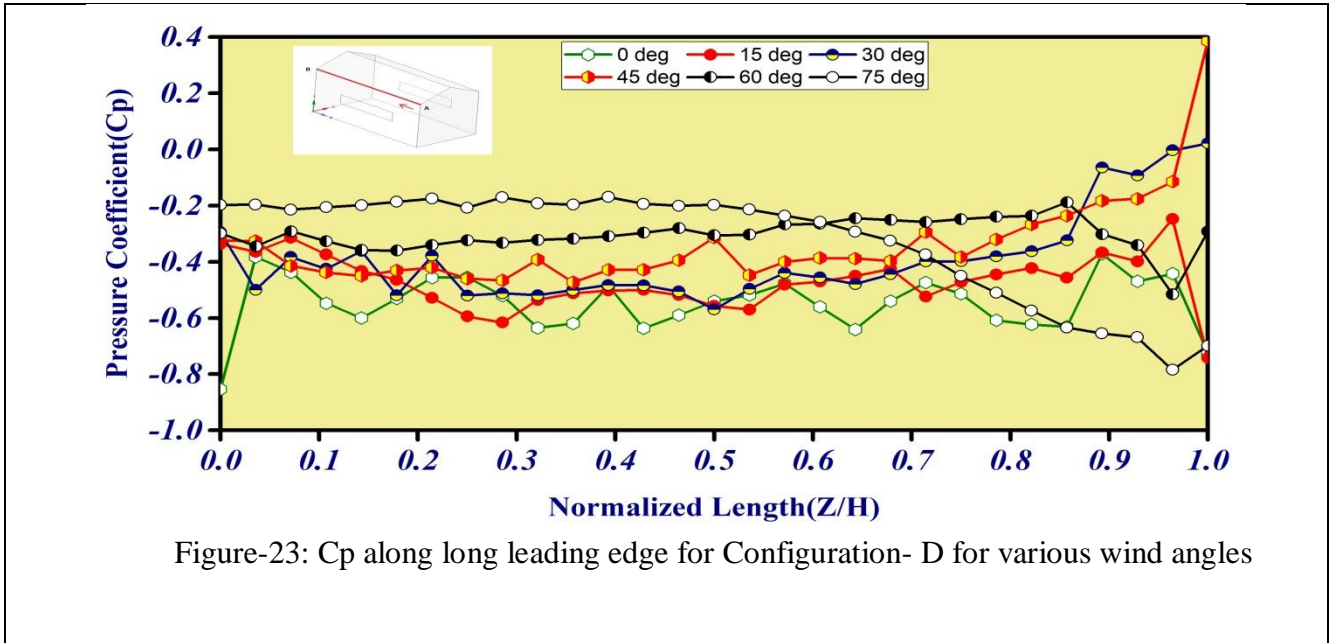
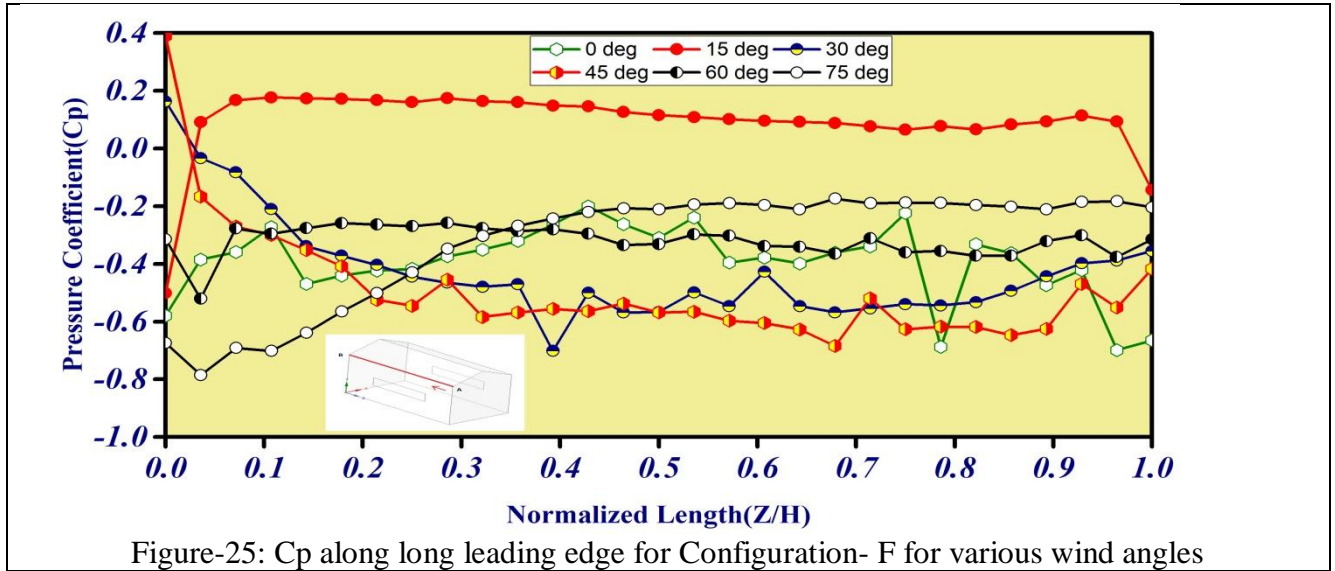


Figure-22: Cp along long leading edge for Configuration- C for various wind angles





5.4 Variation of mean internal pressure -

The internal pressure plays a vital role in case of buildings with openings. The large external suction combined with high positive internal pressure can create a large net load on the building envelope as a result minor to major building envelope failure may occur. The impact of wind incident directions on the internal pressure has been investigated for various configurations. In the Figure 26 the wind directions were plotted in the X-direction and in the Y-direction the mean internal pressure coefficients were considered. It has been observed from the figures that for the configurations A, C and E mean internal coefficient gradually decreases with the change in wind incident angle from 0° to 75°. However, for configurations B and D, it may be noted that the mean internal coefficient of pressure slightly increases as the wind direction changes from 0° to 15° but it decreases gradually as the wind incident angle varies from 15° to 75°. Further, for configuration F, the mean internal pressure coefficient sharply decreases with the change in wind direction from 0° to 15° then it again increases as the wind direction varies from 15° to 30°. The mean internal pressure coefficient then gradually decreases from 30° to 75°.

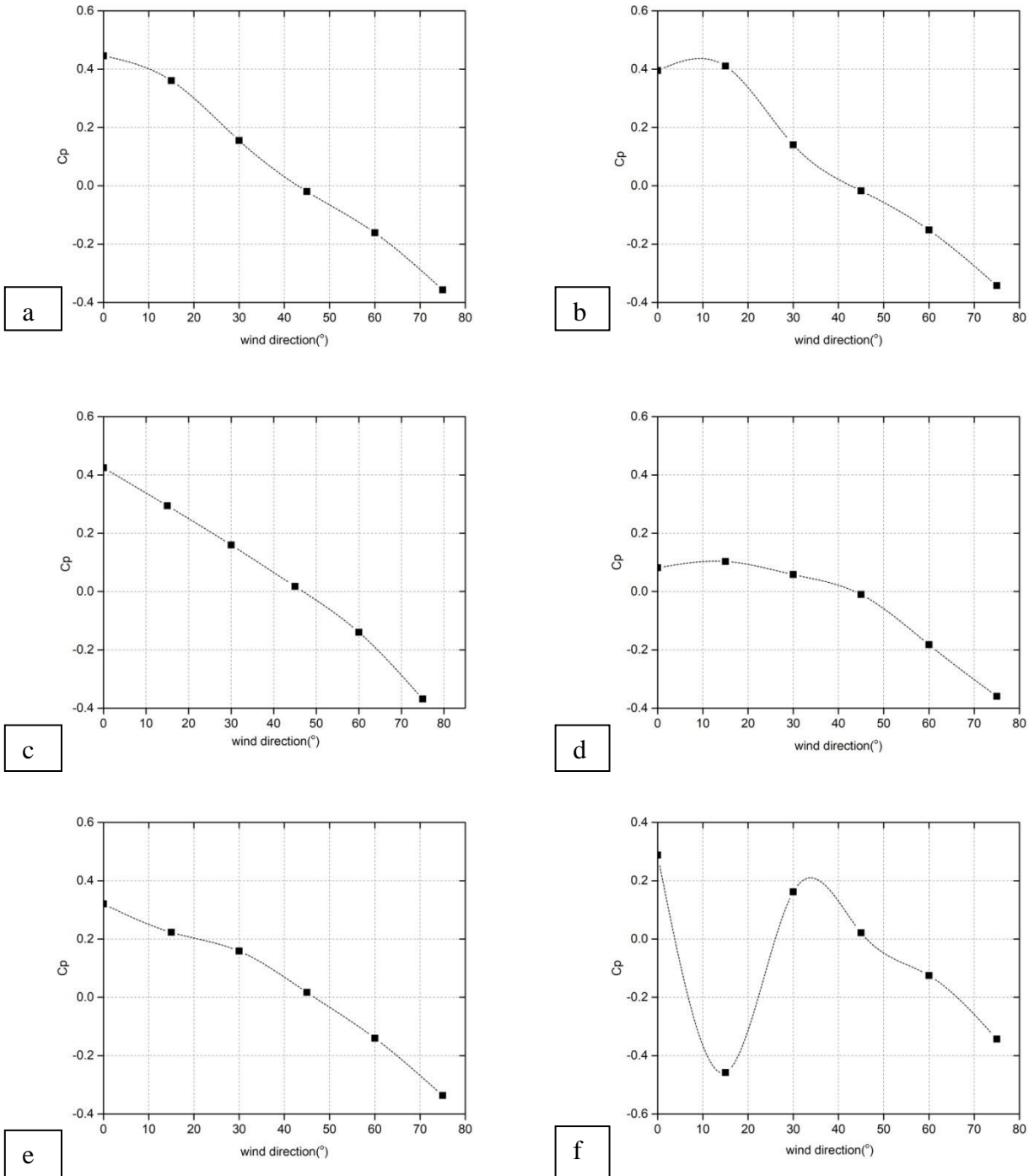


Figure -26 Variation of Mean internal pressures with six different wind incident directions for the configurations -(a) A, (b) B, (c) C, (d) D, (e) E and (f) F

6. Conclusions

The paper presents a CFD analysis to study the flow characteristics of a gable roof building's inner and outer flow fields with six different opening configurations. The steady-state RANS simulations were carried out to investigate the impact of six different wind directions, namely 0° , 15° , 30° , 45° , 60° and 75° on the various building configurations. The main conclusions of this paper are:

- Significant variations in the pressure distribution on the roof of the six building configurations are observed due to the different wind incident angles. As the wind incident angle changes, the location of the roof corner vortices and the intensity of flow separation also change. Hence it can be concluded that the position of the high suction region formed on the roof depends on the wind incident direction and the building configuration.
- The high suction areas on the roof are spread over near the long leading edge and roof ridge. The roof ridge is found to be more significant. The wind incident angle 75° is found to be critical in the case of configuration F for the safety of the roof.
- The mean internal pressure is a function of both the opening configurations and wind directions.

Acknowledgement-

Rupam Deka is currently working as Assistant Professor at the Department of Mechanical Engineering, Dibrugarh University and acknowledges the technical support received from the department.

References

1. Cockroft, J. P., & Robertson, P. (1976). Ventilation of an enclosure through a single opening. *Building and Environment*.11(1):29–35.
2. Eftekhari, M. M. (1995). Single-sided natural ventilation measurements. *Building Services Engineering Research & Technology*.16(4): 221–225.
3. Dascalaki, E., Santamouris, M., Argiriou, A., Helmis, C., Asimakopoulos, D. N., Papadopoulos, K., & Soilemes, A. (1996). On the combination of air velocity and flow measurements in single sided natural ventilation configurations. *Energy and Buildings*. 24(2):155–165.
4. Ginger, J. D., & Letchford, C. W. (1999). Net pressures on a low-rise full-scale building. *Journal of Wind Engineering and Industrial Aerodynamics*. 83(1–3):239–250.
5. Sharma, R. N., & Richards, P. J. (2005). Net pressures on the roof of a low-rise building with wall openings. *Journal of Wind Engineering and Industrial Aerodynamics*.93(4):267–291.
6. Jiang, Y., Alexander, D., Jenkins, H., Arthur, R., & Chen, Q. (2003). Natural ventilation in buildings: Measurement in a wind tunnel and numerical simulation with large-eddy simulation. *Journal of Wind Engineering and Industrial Aerodynamics*. 91(3): 331–353.
7. Karava, P., Stathopoulos, T., & Athienitis, A. K. (2005). Wind driven flow through building openings. Paper presented at International Conference "Passive and Low Energy Cooling for the Built Environment",Greece.
8. Kato, S., Kono, R., Hasama, T., Ooka, R., & Takahashi, T. (2006). A wind tunnel experimental analysis of the ventilation characteristics of a room with single-sided opening in uniform flow. *International Journal of Ventilation*. 5(1): 171–178.

9. Meroney, R. N. (2009). CFD Prediction of Airflow in Buildings for Natural Ventilation. Paper presented at 11th Americas Conference on Wind Engineering, Puerto Rico.
10. Karava, P., Stathopoulos, T., & Athienitis, A. K. (2011). Airflow assessment in cross-ventilated buildings with operable façade elements. *Building and Environment*. 46(1): 266–279.
11. Ramponi, R., & Blocken, B. (2012). CFD simulation of cross-ventilation flow for different isolated building configurations: Validation with wind tunnel measurements and analysis of physical and numerical diffusion effects. *Journal of Wind Engineering and Industrial Aerodynamics*. 104–106: 408–418.
12. Chu, C. R., & Chiang, B. F. (2014). Wind-driven cross ventilation in long buildings. *Building and Environment*. 80:150–158.
13. Perén, J. I., van Hooff, T., Leite, B. C. C., & Blocken, B. (2015). CFD analysis of cross-ventilation of a generic isolated building with asymmetric opening positions: Impact of roof angle and opening location. *Building and Environment*. 85:263–276.
14. Perén, J. I., van Hooff, T., Leite, B. C. C., & Blocken, B. (2016). CFD simulation of wind-driven upward cross ventilation and its enhancement in long buildings: Impact of single-span versus double-span leeward sawtooth roof and opening ratio. *Building and Environment*. 96:142–156.
15. Chu, C. R., Chiu, Y. H., Tsai, Y. T., & Wu, S. L. (2015). Wind-driven natural ventilation for buildings with two openings on the same external wall. *Energy and Buildings*. 108:365–372.
16. Manolesos, M., Gao, Z., & Bouris, D. (2018). Experimental investigation of the atmospheric boundary layer flow past a building model with openings. *Building and Environment*. 141:166–181.
17. Xing, F., Mohotti, D., & Chauhan, K. (2018). Experimental and numerical study on mean pressure distributions around an isolated gable roof building with and without openings. *Building and Environment*, 132:30–44.
18. Yi, Q., König, M., Janke, D., Hempel, S., Zhang, G., Amon, B., & Amon, T. (2018). Wind tunnel investigations of sidewall opening effects on indoor airflows of a cross-ventilated dairy building. *Energy and Buildings*. 175:163–172.
19. Shirzadi, M., Tominaga, Y., & Mirzaei, P. A. (2019). Wind tunnel experiments on cross-ventilation flow of a generic sheltered building in urban areas. *Building and Environment*. 158:60–72.
20. Cao, R., Yu, Z., Liu, Z., Chen, X., & Zhu, F. (2020). Airflow over low-sloped gable roof buildings: Wind tunnel experiment and CFD simulations. *Wind and Structures, An International Journal*. 31(4): 351–362.
21. Franke, J., Hellsten, A., Schlünzen, H., & Carissimo, B. (2007). Best Practice Guideline for the CFD Simulation of Flows in the Urban Environment. Brussels: COST Office 2007.
22. Tominaga, Y., Mochida, A., Yoshie, R., Kataoka, H., Nozu, T., Yoshikawa, M., & Shirasawa, T. (2008). AIJ guidelines for practical applications of CFD to pedestrian wind environment around buildings. *Journal of Wind Engineering and Industrial Aerodynamics*. 96 (10–11):1749–1761.
23. Blocken, B., Stathopoulos, T., & Carmeliet, J. (2007). CFD simulation of the atmospheric boundary layer: wall function problems. *Atmospheric Environment*. 41(2):238–252.